

Synthesis and Fluorescence Properties of Eu³⁺, Tb³⁺ Complexes with Schiff Base Derivatives

Yanhong Liu^{1,2} · Weihua Kong¹ · Zehui Yang³ · Ming Dai¹ · Ling Shi¹ · Dongcai Guo^{1,2}

Received: 30 June 2015 / Accepted: 7 December 2015
© Springer Science+Business Media New York 2015

Abstract Novel Schiff base ligands derived from N'-benzylidene-benzohydrazide (substituted by -H, -CH₃, -OCH₃, -Cl) and 2-chloro-N-phenylacetamide were synthesized. The solid complexes of rare earth (Eu, Tb) nitrate with these Schiff base ligands were synthesized and characterized by elemental analysis, EDTA titrimetric analysis, thermal analysis, infrared spectra and UV-Vis spectra analysis. The fluorescence properties of rare earth (Eu, Tb) complexes in solid were studied. Under the excitation of ultraviolet light, these complexes exhibited characteristic emission of europium and terbium ions. The results showed that the ligand favored energy transfer to the emitting energy of Eu and Tb ions. Effects of different ligands on the fluorescence intensity of rare earth (Eu, Tb) complexes had been discussed. The electrochemical properties of rare earth (Eu, Tb) complexes were also investigated.

Keywords Schiff base · Rare earth complexes · Fluorescence properties

Abbreviations

UV-Vis	Ultraviolet visible
EDTA	Ethylenediaminetetraacetic acid
HOMO	Highest occupied molecular orbital
LUMO	Lowest unoccupied molecular orbital

Introduction

The study of the rare earth complex continues to be an active research area, which is attributed to its application as optical telecommunication devices, as well as biological imaging probes and sensors [1–4], due to characteristic spectroscopic and magnetic properties of rare earth ions. The fluorescence rare earth complexes are of special interest due to their narrow emission bands, a large Stokes' shift. The emission.

mechanism of rare earth ion is based on f–f transition, which results in emission bands with extremely narrow bandwidth and no theoretical cap on the quantum efficiency. The f–f transition forbidden by parity (Laporte) selection rules lead to weak absorbance and low quantum yields, so a suitable chromophoric moiety (antenna) [5–7] is helpful to trigger their emission through efficiently energy transfer from the ligand to the rare earth ion. Our work stems from our interest in the study of coordination behaviors of rare earth ion with Schiff base ligands. Schiff base derivative containing various donor atoms such as nitrogen, oxygen, which enhances the coordination of these ligands with rare earth ions and even yields stable metal complex [8–13].

In this paper, novel Schiff bases ligands have been synthesized, as shown in Scheme 1. The Schiff bases ligands and their complexes have been characterized by FT-IR, ¹H NMR, UV-Vis spectroscopy, elemental analysis. The contribution of

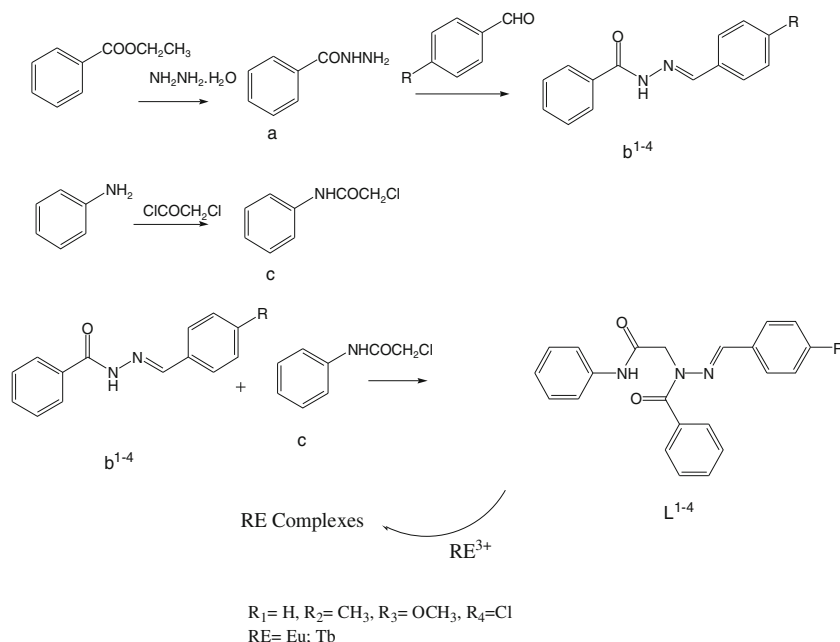
✉ Dongcai Guo
dcguo2001@hnu.edu.cn

¹ School of Chemistry and Chemical Engineering, Hunan University, Changsha 410082, China

² Hunan Provincial Key Laboratory for Cost-effective Utilization of Fossil Fuel Aimed at Reducing Carbon-dioxide Emissions, Changsha 410082, China

³ School of Chemical Engineering, Ningbo University of Technology, Ningbo 315016, China

Scheme 1 The synthetic routes of phenylacetamide derivatives L^{1-4} and rare earth (Eu, Tb) complexes



different ligands to the fluorescence properties can be preliminarily understood.

Experimental Section

Materials and Methods

All the chemicals used were of the analytical grade (AR) and of highest purity.

The rare earth ions were determined by EDTA titration using xylenol oranges as an indicator. Elemental analyses (C, N, and H) was measured on a Vario-EL-III elemental analyzer. The molar conductivity measurements were carried out in acetone using DDS-12A digital direct reading conductivity meter. ^1H NMR and spectra were recorded on a Bruker-400 spectrometer (solvent: $\text{DMSO}-d_6/\text{CDCl}_3$, internal reference: TMS). Mass spectra were recorded on a MAT95XP apparatus. UV-Vis absorption spectra were carried out on a LabTech UV-2100 spectrophotometer. IR spectra were recorded on a PERKIN-ELMER Spectrum One spectrometer by dispersing samples in KBr pellets. Melting points were determined with XT-4 binocular microscopy melting point apparatus. The thermal analysis were performed on a DTG-60 thermal analyzer operating at a heating rate of $20^\circ\text{C}/\text{min}$ in the range of 40°C up to 800°C under in air. Fluorescence spectra were obtained on a HIACHI F-2700 spectrophotometer at a scanning rate of $1500\text{ nm}/\text{min}$, at room temperature, and the voltage was 700 V. The electrochemical properties of the complexes were got by the cyclic voltammetry data on a CHI 660d electrochemical workstation.

General Procedure for Synthesis of Benzohydrazide (a)

Ethyl benzoate (100 mmol, 15.0 g) was dissolved in absolute ethyl alcohol (30 mL) in round bottom flask. Hydrazine hydrate 80 % (20 mL) was added drop wise to the solution and refluxed for 6 h at 80°C . After completion of reaction, the mixture was cooled to rt. for 12 h. The precipitate was filtered, dried and recrystallized in ethanol.

General Procedure for Synthesis of Hydrazones (b^{1-4})

A mixture of (50 mmol, 6.80 g) benzohydrazine (a) and appropriate substituted aromatic aldehyde (50 mmol) was refluxed in ethanol (30 mL) in the presence of a catalytic amount of glacial acetic acid for about 4 h. The progress of the reaction was monitored through TLC. The resulting mixture was cooled to rt. The precipitates obtained was filtered off, washed with ethanol, dried and recrystallized in ethanol to afford the corresponding hydrazone derivatives. Structures of the synthesized compounds were confirmed on the basis of spectral data.

N'-benzylidene-benzohydrazide (b^1) White solid, Yield 90 %, ^1H NMR (400 MHz, $\text{DMSO}-d_6$) δ /ppm: 11.82 (s, 1 H, $\text{CH} = \text{N}$), 8.47 (s, 1 H, NH), 7.92 (d, $J = 7.1\text{ Hz}$, 2 H, ArH), 7.73 (s, 2 H, ArH), 7.63–7.56 (m, 1 H, ArH), 7.52 (d, $J = 14.1\text{ Hz}$, 2 H, ArH), 7.46 (d, $J = 6.3\text{ Hz}$, 3 H, ArH); MS (EI) m/z (%): 225 ($m + 1$, 1), 224 (m , 5), 223 ($m - 1$, 1), 123 (1), 122 (3), 121 (36), 105 (100), 103 (4), 77 (32), 65 (4), 51 (9).

N'-(4-methylbenzylidene)benzohydrazide (b^2) White solid, Yield 87 %, ^1H NMR (400 MHz, $\text{DMSO}-d_6$) δ /ppm: 11.77 (s, 1 H, $\text{CH} = \text{N}$), 8.42 (s, 1 H, NH), 7.91 (d,

$J = 7.4$ Hz, 2 H, ArH), 7.63 (d, $J = 7.9$ Hz, 2 H, ArH), 7.58 (d, $J = 7.0$ Hz, 1 H, ArH), 7.52 (t, $J = 7.4$ Hz, 2 H, ArH), 7.28 (d, $J = 7.7$ Hz, 2 H, ArH), 2.35 (s, 3 H, CH₃); MS (EI) m/z (%): 239 ($m + 1$, 2), 238 (m , 9), 237 ($m - 1$, 1), 121 (2), 105 (100), 78 (6), 77 (34), 76 (2), 51 (5).

N'-(4-methoxybenzylidene)benzohydrazide (**b**³) White solid, Yield 89 %, ¹H NMR (400 MHz, DMSO-*d*₆) δ /ppm: 11.70 (s, 1 H, CH = N), 8.40 (s, 1 H, NH), 7.90 (d, $J = 7.5$ Hz, 2 H, ArH), 7.68 (d, $J = 8.5$ Hz, 2 H, ArH), 7.61–7.55 (m, 1 H, ArH), 7.52 (t, $J = 7.3$ Hz, 2 H, ArH), 7.03 (d, $J = 8.5$ Hz, 2 H, ArH), 3.81 (s, 3 H, OCH₃); MS (EI) m/z (%): 256 ($m + 2$, 1), 255 ($m + 1$, 3), 254 (m , 16), 135 (3), 134 (14), 133 (100), 106 (9), 105 (92), 78 (5), 77 (38), 76 (5), 51 (7).

N'-(4-chlorobenzylidene)benzohydrazide (**b**⁴) White solid, Yield 82 %, ¹H NMR (400 MHz, DMSO-*d*₆) δ /ppm: 11.90 (s, 1 H, CH = N), 8.45 (s, 1 H, NH), 7.91 (d, $J = 7.3$ Hz, 2 H, ArH), 7.76 (d, $J = 8.0$ Hz, 2 H, ArH), 7.59 (d, $J = 7.1$ Hz, 1 H, ArH), 7.52 (d, $J = 6.0$ Hz, 4 H, ArH); MS (EI) m/z (%): 261 ($m + 3$, 1), 260 ($m + 2$, 6), 258 (m , 14), 257 ($m - 1$, 2), 121 (37), 105 (100), 90 (2), 89 (5), 77 (25), 63 (3), 51 (4).

General Procedure for Synthesis of 2-Chloro-N-Phenylacetamide (**c**)

Aniline (50 mmol, 4.65 g) was dissolved in glacial acetic acid (40 mL), the solution was cooled in ice bath with stirring. Chloroacetylchloride (50 mmol, 5.60 g) was added dropwise to avoid the vigorous reaction. After 0.5 h, it was moved to react at room temperature for 1 h. Then it was poured to 200 mL saturated solution of sodium acetate. The precipitate was filtered, washed with water, recrystallized from alcohol-water solution to afford white product. Yield 87 %.

General Procedure for Synthesis of Ligands **L**^{1–4}

Hydrazones (**b**^{1–4}) (20 mmol), anhydrous K₂CO₃ (50 mmol, 6.90 g) and dimethyl formamide (20 mL) were warmed to 85 °C, then 2-chloro-N-phenylacetamide (**c**) (20 mmol, 3.38 g) in dimethyl formamide (10 mL) and a little KI were added slowly. The mixture was refluxed for 3 h. After cooling down, it was poured into distilled water (300 mL), and then diluted hydrochloric acid (2 mol/L) was added until the pH value was 3–4 for a further 10 min. The crude final product was filtered with suction, washed several times with cold water, and dried. The crude product was dissolved in appropriate dichloromethane, filtered, washed with a little dichloromethane and recrystallized from suitable solvents to obtain white flocculent solids [15]. The yield, melting point, and spectral data of each compound are given below.

2-(N-Benzoyl-N'-benzylidene-hydrazino)-N-phenylacetamide (**L**¹) Yield 64 %, m.p. 147–148 °C; ¹H NMR

(400 MHz, CDCl₃) δ /ppm: 8.61 (s, 1 H, CH = N), 8.19 (s, 1 H, NH), 7.88 (d, $J = 7.3$ Hz, 2 H, ArH), 7.59–7.45 (m, 7 H, ArH), 7.38–7.30 (m, 5 H, ArH), 7.12 (t, $J = 7.4$ Hz, 1 H, ArH), 4.94 (s, 2 H, CH₂); IR (KBr) ν /cm⁻¹: 3283, 2361, 1691, 1632, 1612, 1556, 1447, 1423, 1348, 1136, 1078, 754, 690; MS (EI) m/z (%): 358 ($m + 1$, 3), 357 (m , 8), 267 (1), 266 (5), 265 (28), 135 (1), 134 (5), 106 (9), 105 (100), 93 (24), 89 (6), 77 (35), 76 (3), 51 (6); Anal. Calcd for C₂₂H₁₉N₃O₂: C, 73.93; H, 5.36; N, 11.76. Found: C, 73.78; H, 5.26; N, 11.89.

2-(N-Benzoyl-N'-benzylidene-hydrazino)-N-p-tolylacetamide (**L**²) Yield 54 %, m.p. 151–153 °C; ¹H NMR (400 MHz, CDCl₃) δ /ppm: 8.65 (s, 1 H, CH = N), 8.16 (s, 1 H, NH), 7.88 (d, $J = 7.4$ Hz, 2 H, ArH), 7.50 (ddd, $J = 26.7$, 16.6, 7.7 Hz, 7 H, ArH), 7.32 (t, $J = 7.6$ Hz, 2 H, ArH), 7.13 (dd, $J = 17.0$, 7.6 Hz, 3 H, ArH), 4.93 (s, 2 H, CH₂), 2.35 (s, 3 H, CH₃); IR (KBr) ν /cm⁻¹: 3283, 2359, 1691, 1632, 1614, 1556, 1446, 1427, 1346, 1138, 1078, 752, 692; MS (EI) m/z (%): 372 ($m + 1$, 3), 371 (m , 12), 281 (1), 280 (5), 279 (16), 119 (8), 118 (12), 105 (100), 93 (32), 91 (7), 77 (31), 65 (4); Anal. Calcd for C₂₃H₂₁N₃O₂: C, 74.37; H, 5.70; N, 11.31. Found: C, 74.21; H, 5.64; N, 11.50.

2-(N-Benzoyl-N'-benzylidene-hydrazino)-N-(4-methoxyphenyl)-acetamide (**L**³) Yield 62 %, m.p. 143–144 °C; ¹H NMR (400 MHz, CDCl₃) δ /ppm: 8.67 (s, 1 H, CH = N), 8.15 (s, 1 H, NH), 7.87 (d, $J = 7.3$ Hz, 2 H, ArH), 7.58–7.44 (m, 7 H, ArH), 7.32 (t, $J = 7.9$ Hz, 2 H, ArH), 7.12 (t, $J = 7.4$ Hz, 1 H, ArH), 6.87 (d, $J = 8.7$ Hz, 2 H, ArH), 4.92 (s, 2 H, CH₂), 3.81 (s, 3 H, CH₃); IR (KBr) ν /cm⁻¹: 3277, 2363, 1687, 1636, 1609, 1556, 1446, 1429, 1350, 1136, 1080, 758, 694; MS (EI) m/z (%): 388 ($m + 1$, 2), 387 (m , 7), 296 (1), 295 (6), 135 (15), 134 (14), 133 (17), 120 (18), 105 (100), 93 (37), 91 (12), 65 (6), 51 (10); Anal. Calcd for C₂₃H₂₁N₃O₃: C, 71.30; H, 5.46; N, 10.85. Found: C, 71.14; H, 5.36; N, 10.89.

2-(N-Benzoyl-N'-benzylidene-hydrazino)-N-(4-chlorophenyl)-acetamide (**L**⁴) Yield 72 %, m.p. 151–152 °C; ¹H NMR (400 MHz, CDCl₃) δ /ppm: 8.62 (s, 1 H, CH = N), 8.16 (s, 1 H, NH), 7.90–7.77 (m, 2 H, ArH), 7.52 (ddd, $J = 19.9$, 16.6, 8.1 Hz, 7 H, ArH), 7.38–7.27 (m, 4 H, ArH), 7.12 (t, $J = 7.4$ Hz, 1 H, ArH), 4.92 (s, 2 H, CH₂); IR (KBr) ν /cm⁻¹: 3287, 2372, 1699, 1638, 1612, 1556, 1447, 1427, 1342, 1140, 1089, 754, 696; MS (EI) m/z (%): 393 ($m + 2$, 2), 391 (m , 4), 302 (1), 301 (6), 299 (19), 298 (1), 106 (9), 105 (100), 93 (16), 89 (3), 77 (27), 51 (4); Anal. Calcd for C₂₂H₁₈ClN₃O₂: C, 67.43; H, 4.63; N, 10.72. Found: C, 67.31; H, 4.57; N, 10.86.

Preparation of the Complexes

An ethanol solution (5 mL) of RE(NO₃)₃·6H₂O (RE = Eu, Tb) (1 mmol) was added dropwise to a solution of 1 mmol ligand **L**^{1–4} in the chloroform (30 mL). The mixture was refluxed at 80 °C for 4 h. And then the pH value

Table 1 Elementary analysis and conductivity data of Eu(III), Tb(III) complexes

Complex	Measured value (Theoretical value %)				Λ_m ($S \cdot cm^2 \cdot mol^{-1}$)
	C	H	N	RE	
[Eu(NO ₃) ₂ L ¹]NO ₃ ·2H ₂ O	36.01 (36.11)	3.06 (3.15)	11.23 (11.49)	20.85 (20.79)	70
[Eu(NO ₃) ₂ L ²]NO ₃ ·2H ₂ O	36.87 (37.05)	3.19 (3.35)	11.05 (11.27)	20.52 (20.40)	72
[Eu(NO ₃) ₂ L ³]NO ₃ ·2H ₂ O	36.12 (36.27)	3.05 (3.28)	10.94 (11.04)	20.23 (19.97)	75
[Eu(NO ₃) ₂ L ⁴]NO ₃ ·2H ₂ O	34.46 (34.51)	2.75 (2.87)	10.84 (10.98)	19.98 (19.87)	81
[Tb(NO ₃) ₂ L ¹]NO ₃ ·2H ₂ O	35.66 (35.77)	3.09 (3.12)	11.23 (11.38)	21.75 (21.54)	77
[Tb(NO ₃) ₂ L ²]NO ₃ ·2H ₂ O	36.54 (36.70)	3.19 (3.32)	11.05 (11.17)	21.32 (21.14)	72
[Tb(NO ₃) ₂ L ³]NO ₃ ·2H ₂ O	35.82 (35.93)	3.15 (3.25)	10.84 (10.94)	20.83 (20.70)	75
[Tb(NO ₃) ₂ L ⁴]NO ₃ ·2H ₂ O	34.16 (34.20)	2.85 (2.85)	10.84 (10.88)	20.51 (20.59)	75

was adjusted to 6.0–6.5 by a solution of sodium ethoxide in ethanol (1 mol/L). The precipitated solid complex was filtered, washed with hot chloroform, dried in vacuum for 48 h.

Results and Discussion

Properties of Target Complexes

Analytical data for the complexes, presented in Table 1, indicated that the nitrate complexes conformed to a 1:1 metal-to-ligand stoichiometry [RE(NO₃)₃L^{1–4}]·2H₂O. The compounds L^{1–4} were white powers and soluble in dichloromethane, all the nitrate complexes were white powers and slightly soluble in DMSO, DMF, insoluble in benzene and diethyl ether. The molar conductance data of these complexes in DMF solution ($1 \times 10^{-3} \text{ mol} \cdot \text{L}^{-1}$) was in the range of 70–81 $S \cdot cm^2 \cdot mol^{-1}$, which indicated that all complexes

are 1:1 ionic compounds [20]. From the analyses above, composition of the complexes can be inferred: [RE(NO₃)₂L^{1–4}]NO₃·2H₂O (RE = Eu, Tb).

IR Spectral Analyses

The main IR peaks of the ligands and their Eu(III), Tb(III) complexes are presented in Table 2. From Figs. 1 and 2, the IR spectrum of the free ligand L⁴ showed strong absorption band at 1699 cm^{-1} , which was assigned to the stretch vibration of the carbonyl group [$\nu(C=O)$]. In the nitrate complexes, the red shifts to about 1653 cm^{-1} ($\Delta\nu = 46 \text{ cm}^{-1}$) and 1647 cm^{-1} ($\Delta\nu = 52 \text{ cm}^{-1}$) in [Eu(NO₃)₂L⁴]NO₃·2H₂O, 1647 cm^{-1} ($\Delta\nu = 52 \text{ cm}^{-1}$) and 1636 cm^{-1} ($\Delta\nu = 63 \text{ cm}^{-1}$) in [Tb(NO₃)₂L⁴]NO₃·2H₂O, indicating that the oxygen atom of C=O and N–C=O took part in coordination to RE (Eu³⁺, Tb³⁺) ions, respectively. It resulted in the equalization of electron cloud on the C=O group, then the absorption frequencies moved to the low wave number due to the decrease of the

Table 2 IR data (cm^{-1}) of ligands L^{1–4} and their Eu(III), Tb(III) complexes

Compounds	$\nu(O-H)$	$\nu(N-C=O)$	$\nu(C=O)$	$\nu(NO_3^-)$					
				ν_1	ν_2	ν_3	ν_4	ν	$ \nu_1 - \nu_4 $
L ¹		2361	1691						
[Eu(NO ₃) ₂ L ¹]NO ₃ ·2H ₂ O	3524	2359	1653, 1647	1456	1041	835	1362	1385	94
[Tb(NO ₃) ₂ L ¹]NO ₃ ·2H ₂ O	3524	2357	1651, 1645	1456	1045	835	1362	1385	94
L ²		2359	1691						
[Eu(NO ₃) ₂ L ²]NO ₃ ·2H ₂ O	3524	2360	1653, 1647	1458	1041	837	1362	1385	96
[Tb(NO ₃) ₂ L ²]NO ₃ ·2H ₂ O	3524	2355	1651, 1645	1456	1043	835	1362	1385	94
L ³		2363	1687						
[Eu(NO ₃) ₂ L ³]NO ₃ ·2H ₂ O	3524	2359	1653, 1647	1456	1041	837	1362	1385	94
[Tb(NO ₃) ₂ L ³]NO ₃ ·2H ₂ O	3500	2355	1651, 1645	1454	1041	835	1362	1385	92
L ⁴		2372	1699						
[Eu(NO ₃) ₂ L ⁴]NO ₃ ·2H ₂ O	3503	2360	1653, 1647	1456	1041	835	1362	1385	94
[Tb(NO ₃) ₂ L ⁴]NO ₃ ·2H ₂ O	3524	2359	1647, 1636	1456	1041	835	1362	1385	94

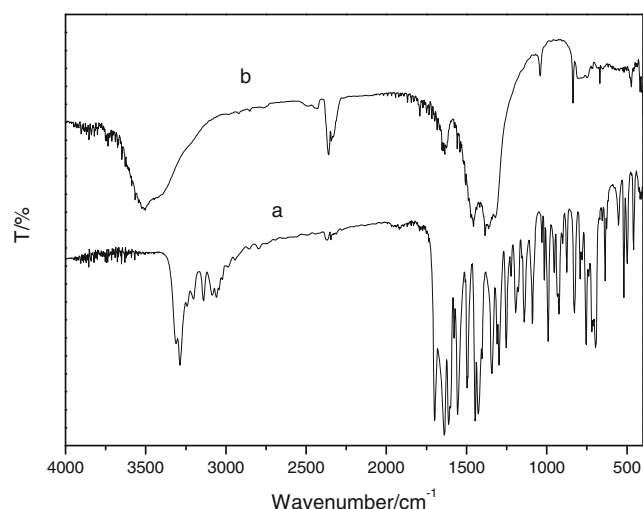


Fig. 1 IR spectra of the ligand L^4 (a) and the complex $[EuL^4(NO_3)_2]NO_3 \cdot 2H_2O$ (b)

force constant. Meanwhile, the stretch vibration of triple bond $[\nu(N-C=O)]$ shifted from 2372 cm^{-1} in L^4 to 2360 cm^{-1} in $[Eu(NO_3)_2L^4]NO_3 \cdot 2H_2O$ ($\Delta\nu = 8\text{ cm}^{-1}$), and to 2359 cm^{-1} in $[Tb(NO_3)_2L^4]NO_3 \cdot 2H_2O$ ($\Delta\nu = 13\text{ cm}^{-1}$), respectively. This was also confirmed that the oxygen of $N-C=O$ was involved in the coordination.

The characteristic frequencies of the coordinating nitrate groups (C_{2v}) in $[Eu(NO_3)_2L^4]NO_3 \cdot 2H_2O$ and $[Tb(NO_3)_2L^4]NO_3 \cdot 2H_2O$ both appeared at about 1456 cm^{-1} (ν_1), 1041 cm^{-1} (ν_2), 835 cm^{-1} (ν_3), and 1362 cm^{-1} (ν_4) and the difference between the two highest frequency bands ($|\nu_1 - \nu_4|$) was 94 cm^{-1} , indicating that the coordinated nitrate groups in the complexes were bidentate state [14, 19, 21]. The free nitrate groups (D_{3h}) appeared at ca. 1385 cm^{-1} in the spectra of the complexes, which explained that one nitrate group can not participate in the coordination. Additionally, broad bands at

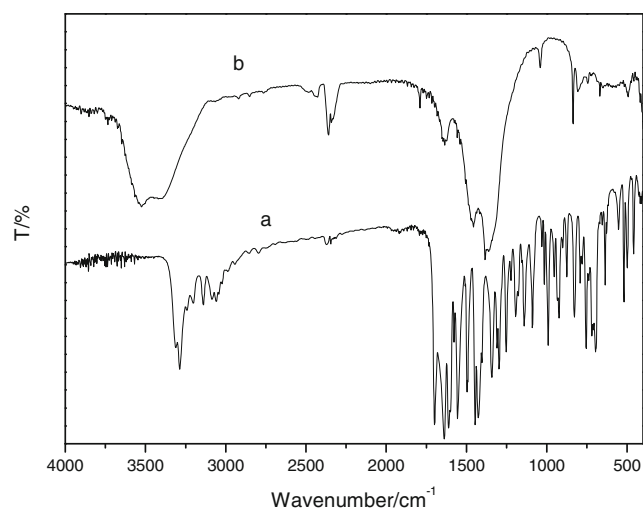


Fig. 2 IR spectra of the ligand L^4 (a) and the complex $[TbL^4(NO_3)_2]NO_3 \cdot 2H_2O$ (b)

Table 3 UV-Vis spectra data of ligands L^{1-4} and their Eu(III), Tb(III) complexes

compounds	λ_1 (nm)	λ_2 (nm)
L^1	267	298
$[Eu(NO_3)_2L^1]NO_3 \cdot 2H_2O$	265	— ^a
$[Tb(NO_3)_2L^1]NO_3 \cdot 2H_2O$	266	—
L^2	268	302
$[Eu(NO_3)_2L^2]NO_3 \cdot 2H_2O$	266	—
$[Tb(NO_3)_2L^2]NO_3 \cdot 2H_2O$	264	—
L^3	266	305
$[Eu(NO_3)_2L^3]NO_3 \cdot 2H_2O$	265	—
$[Tb(NO_3)_2L^3]NO_3 \cdot 2H_2O$	267	—
L^4	268	305
$[Eu(NO_3)_2L^4]NO_3 \cdot 2H_2O$	265	—
$[Tb(NO_3)_2L^4]NO_3 \cdot 2H_2O$	264	—

^a—, No absorption peak

3503 cm^{-1} in $[Eu(NO_3)_2L^4]NO_3 \cdot 2H_2O$ and 3524 cm^{-1} in $[Tb(NO_3)_2L^4]NO_3 \cdot 2H_2O$ indicated that H_2O were existent in Eu(III) and Tb(III) complexes, confirming the elemental analysis. These results confirmed that the coordination bond was formed between the ligand L^4 and the Eu(III), Tb(III) ions, respectively.

UV-Vis Spectral Analyses

UV-vis spectra of rare earth complexes (Eu, Tb) and their corresponding Schiff base ligands were recorded in DMSO solution ($1 \times 10^{-5}\text{ mol} \cdot \text{L}^{-1}$), the data are listed in Table 3. Two absorption peaks of the free ligand L^4 appeared at 268 and 305 nm, which were assigned to the $\pi \rightarrow \pi^*$ and $n \rightarrow \pi^*$ transitions of the ligand, as shown in Fig. 3. However, the first strong absorption wavelength of $[Eu(NO_3)_2L^4]NO_3 \cdot 2H_2O$ was 265 nm, while the second was disappeared. This was

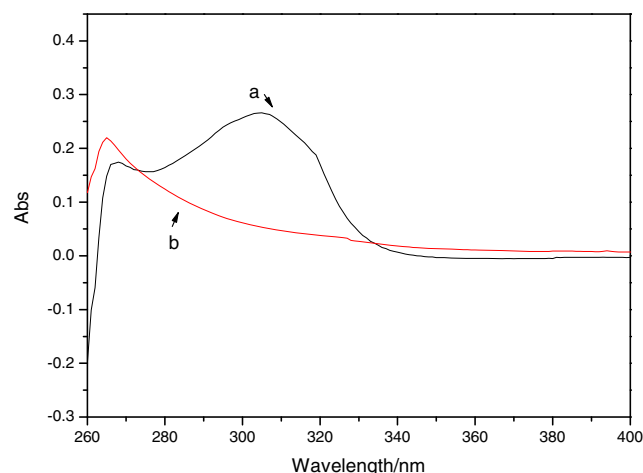


Fig. 3 UV-Vis spectra of L^4 (a) and $[Eu(NO_3)_2L^4]NO_3 \cdot 2H_2O$ (b)

Table 4 TG-DTA data of Eu(III), Tb(III) complexes

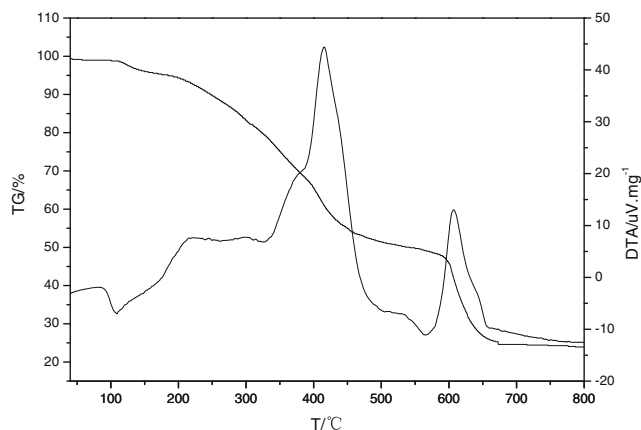
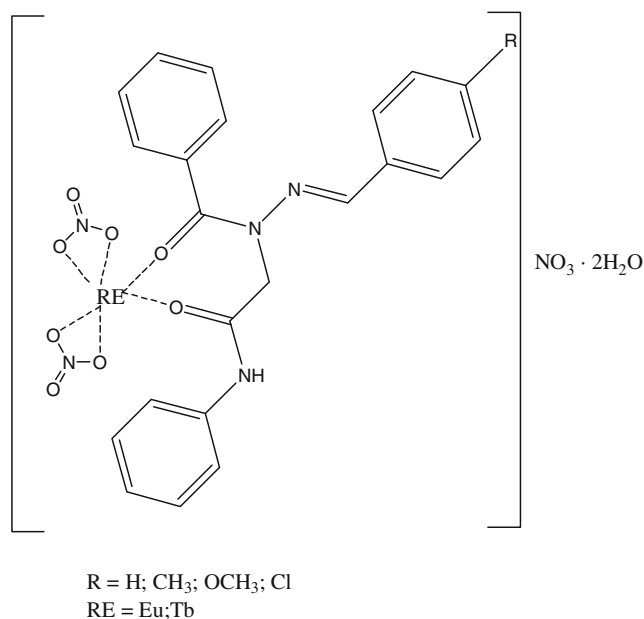
Complexes	Endothermic Peak(°C)	Exothermic Peak(°C)	Residual Weight (Theoretical Value)(%)
[Eu(NO ₃) ₂ L ¹](NO ₃)·2H ₂ O	109, 566	415, 607	24.09 (24.08)
[Eu(NO ₃) ₂ L ²](NO ₃)·2H ₂ O	110, 567	418, 610	23.11 (23.62)
[Eu(NO ₃) ₂ L ³](NO ₃)·2H ₂ O	106, 571	420, 617	29.84 (23.13)
[Eu(NO ₃) ₂ L ⁴](NO ₃)·2H ₂ O	117, 574	418, 620	29.79 (23.01)
[Tb(NO ₃) ₂ L ¹](NO ₃)·2H ₂ O	103, 569	411, 618	25.01 (25.34)
[Tb(NO ₃) ₂ L ²](NO ₃)·2H ₂ O	100, 571	417, 619	24.51 (24.87)
[Tb(NO ₃) ₂ L ³](NO ₃)·2H ₂ O	106, 576	420, 621	24.48 (24.35)
[Tb(NO ₃) ₂ L ⁴](NO ₃)·2H ₂ O	107, 573	416, 611	24.17 (24.22)

because that the steady coordinate bond changed the distribution of electron cloud.

Thermal Analyses

Thermal properties were evaluated by means of DTA and TG in air. The results are presented in Table 4. Figure 4 showed that the [Eu(NO₃)₂L¹](NO₃)·2H₂O started to decompose at 100–180 °C, and the mass loss (4.83 %) was match well with the theoretical value (4.92 %), indicating that there were two H₂O molecules in the complex. The TG graph showed that the ligand L¹ was lost at 200–480 °C, and the mass loss (42.71 %) was in according to the theoretical value (48.84 %). Three NO₃[−] were lost at 480–661 °C accompanying with exothermic peaks at 607 °C. The experimental mass loss (26.64 %) was close to the calculated value (25.44 %). When the complex was completely decomposed into rare earth oxide, the residual weigh was 24.08 %, which was very close to the experimental result (24.09 %).

From the analyses (IR spectra, elemental analysis, and thermodynamic analysis) above we can deduce the composition and molecular structure of the complexes, as shown in Fig. 5.

**Fig. 4** TG-DTA of [Eu(NO₃)₂L¹](NO₃)·2H₂O**Fig. 5** The molecular structure of rare earth (Eu, Tb) complexes

Fluorescence Properties

The fluorescence properties of the ligand and rare earth (Eu, Tb) complexes are investigated. The excitation and emission spectra of all the samples were measured at room temperature in the solid state. The results are presented in Tables 5, 6, 7 and Figs. 6, 7 and 8.

Under the excitation of UV light, the L¹⁻⁴ exhibited blue light. From Fig. 6, it was obvious that peaks shape were similar to each other, the excitation wavelength of the ligand was 338.0 nm, and emission intensity was decreased in the order L¹ > L⁴ > L² > L³. The fluorescence intensity of the ligands L²⁻⁴ were decreased, mainly due to the effects of substituent (−CH₃, −OCH₃, −Cl) on the fluorescence quantum efficiency. The substituent changed the conjugated π-system, and the smaller the π-system, the weaker the fluorescence intensity. Importantly, the substituent decreased molecular rigidity and increased the molecular vibration, thus it enhanced the probability of deactivation due to the collisions with

Table 5 Fluorescence spectral data of ligands L¹⁻⁴

Compound	Ex Slit (nm)	Em Slit (nm)	λ _{ex} ^a (nm)	λ _{em} ^b (nm)	RLI ^c
L ¹	2.5	2.5	338.0	435.0	6483
L ²	2.5	2.5	338.0	443.5	2058
L ³	2.5	2.5	338.0	439.5	1792
L ⁴	2.5	2.5	338.0	430.0	2389

^a The maximum fluorescence excitation wavelength

^b The fluorescence characteristic emission wavelength

^c Relative fluorescence intensity

Table 6 Fluorescence spectral data of Eu (III) complexes

Compound	Ex Slit (nm)	Em Slit (nm)	$\lambda_{\text{ex}}^{\text{a}}$ (nm)	$\lambda_{\text{em}}^{\text{b}}$ (nm)	RLI ^c	Assignment
[Eu(NO ₃) ₂ L ¹][NO ₃ ·2H ₂ O]	5.0	2.5	396.0	595.0	1412	⁵ D ₀ → ⁷ F ₁
				618.5	1184	⁵ D ₀ → ⁷ F ₂
[Eu(NO ₃) ₂ L ²][NO ₃ ·2H ₂ O]	5.0	2.5	396.0	595.0	1733	⁵ D ₀ → ⁷ F ₁
				618.5	1462	⁵ D ₀ → ⁷ F ₂
[Eu(NO ₃) ₂ L ³][NO ₃ ·2H ₂ O]	5.0	2.5	396.0	595.0	1316	⁵ D ₀ → ⁷ F ₁
				618.5	1143	⁵ D ₀ → ⁷ F ₂
[Eu(NO ₃) ₂ L ⁴][NO ₃ ·2H ₂ O]	5.0	2.5	396.0	595.0	2287	⁵ D ₀ → ⁷ F ₁
				618.5	1859	⁵ D ₀ → ⁷ F ₂

^a The maximum fluorescence excitation wavelength^b The fluorescence characteristic emission wavelength^c Relative fluorescence intensity

other molecules, and decreased the fluorescence quantum efficiency.

From Table 6 and Fig. 7, peaks shape of all Eu(III) complexes were similar to each other. The excitation wavelength of all complexes were at 396.0 nm, the emission wavelength at 595.0 and 618.5 nm, which were assigned to the magnetic dipole transition (⁵D₀ → ⁷F₁) and electric dipole transition (⁵D₀ → ⁷F₂) of the Eu³⁺ ion. The magnetic dipole transition (⁵D₀ → ⁷F₁) was independent of the ligand environment, while the electric dipole transition (⁵D₀ → ⁷F₂) was sensitive to the surrounding electric field. As shown in Fig. 5, the emission intensity of the ⁵D₀ → ⁷F₂ transition was weaker than that

of the ⁵D₀ → ⁷F₁, and the ratio (⁵D₀ → ⁷F₂/⁵D₀ → ⁷F₁) of the complexes [Eu(NO₃)₂L¹⁻⁴][NO₃·2H₂O] were 0.77, 0.85, 0.87, 0.81. Thus, the central Eu³⁺ ion was located in a symmetric coordination site [18].

As shown in Table 7 and Fig. 8, the excitation wavelength of all complexes were at 370.0 nm, the characteristic emission peaks were assigned to the ⁵D₄ → ⁷F_j (j = 3, 4, 5, 6) of the central Tb³⁺ ion. As for [Tb(NO₃)₂L⁴][NO₃·2H₂O], the main band of Tb (III) ion at 491.0 nm, 546.5 nm, 586.5 nm, and 623.5 nm, was assigned to the ⁵D₄ → ⁷F₆, ⁵D₄ → ⁷F₅, ⁵D₄ → ⁷F₄, ⁵D₄ → ⁷F₃ transition, respectively. The emission intensity at 546.5 nm from the electric dipole transition

Table 7 Fluorescence spectral data of Tb (III) complexes

Compound	Ex Slit (nm)	Em Slit (nm)	$\lambda_{\text{ex}}^{\text{a}}$ (nm)	$\lambda_{\text{em}}^{\text{b}}$ (nm)	RLI ^c	Assignment
[Tb(NO ₃) ₂ L ¹][NO ₃ ·2H ₂ O]	5.0	2.5	370.0	491.0	1231	⁵ D ₄ → ⁷ F ₆
				547.5	1099	⁵ D ₄ → ⁷ F ₅
				586.0	657.0	⁵ D ₄ → ⁷ F ₄
				623.5	587.0	⁵ D ₄ → ⁷ F ₃
[Tb(NO ₃) ₂ L ²][NO ₃ ·2H ₂ O]	5.0	2.5	370.0	491.0	3621	⁵ D ₄ → ⁷ F ₆
				547.5	4883	⁵ D ₄ → ⁷ F ₅
				586.5	1170	⁵ D ₄ → ⁷ F ₄
				623.5	658.3	⁵ D ₄ → ⁷ F ₃
[Tb(NO ₃) ₂ L ³][NO ₃ ·2H ₂ O]	5.0	2.5	370.0	491.0	1449	⁵ D ₄ → ⁷ F ₆
				546.0	1427	⁵ D ₄ → ⁷ F ₅
				586.5	703.0	⁵ D ₄ → ⁷ F ₄
				622.5	570.9	⁵ D ₄ → ⁷ F ₃
[Tb(NO ₃) ₂ L ⁴][NO ₃ ·2H ₂ O]	5.0	2.5	370.0	491.0	6712	⁵ D ₄ → ⁷ F ₆
				546.5	... ^d	⁵ D ₄ → ⁷ F ₅
				586.5	1997	⁵ D ₄ → ⁷ F ₄
				623.5	803.2	⁵ D ₄ → ⁷ F ₃

^a The maximum fluorescence excitation wavelength^b The fluorescence characteristic emission wavelength^c Relative fluorescence intensity^d ..., the numeral of relative intensity is larger than 10,000

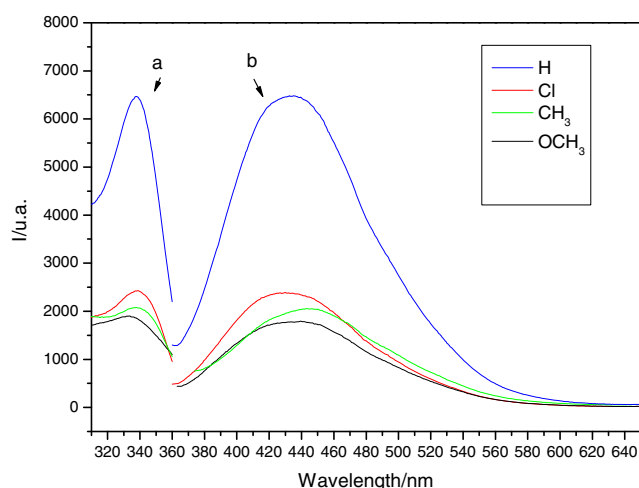


Fig. 6 Excitation (a) and emission (b) spectra of ligand L^{1-4}

($^5D_4 \rightarrow ^7F_5$) was strongest, which deduced that the Tb (III) ion was located in an asymmetric coordination site. The strongest emission peaks of all complexes were different, which indicated that the ligand had different influence on the coordination environment. Among all Tb(III) complexes, the ratio of emission intensity ($^5D_4 \rightarrow ^7F_5$, $^5D_4 \rightarrow ^7F_6$) were 0.89, 1.39, 0.98, 1.49, which explained that the Tb^{3+} ions in $[Tb(NO_3)_2 L^{1,3}]NO_3 \cdot 2H_2O$ were in the center of symmetry, but $[Tb(NO_3)_2 L^{2,4}]NO_3 \cdot 2H_2O$ conversely.

Figures 7, and 8 showed that the emission peak of the ligand L^{1-4} at 430–443 nm were disappeared, and the emission intensity of RE (Eu, Tb) complexes were decreased in the order $[RE(NO_3)_2 L^4]NO_3 \cdot 2H_2O > [RE(NO_3)_2 L^2]NO_3 \cdot 2H_2O > [RE(NO_3)_2 L^3]NO_3 \cdot 2H_2O > [RE(NO_3)_2 L^1]NO_3 \cdot 2H_2O$. Obviously, the ligand transferred energy to the central ion, the fluorescence of rare earth complexes were attributed to the efficient intra-molecular energy transfer from the triplet state level of the ligands (L^{1-4}) to the lowest excited state level

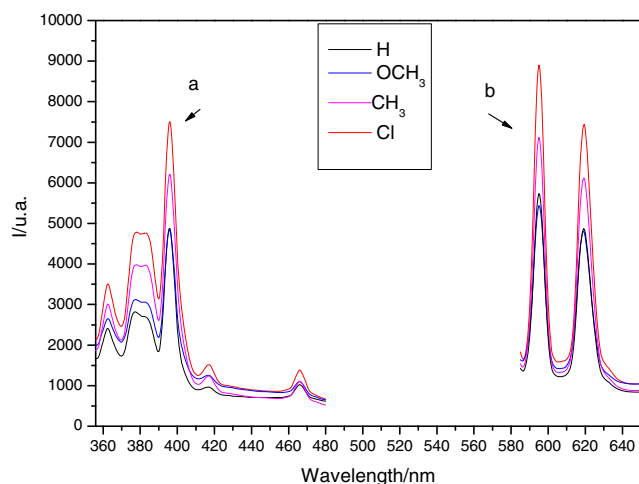


Fig. 7 Excitation (a) and emission (b) spectra of the complexes $[Eu(NO_3)_2 L^{1-4}]NO_3 \cdot 2H_2O$

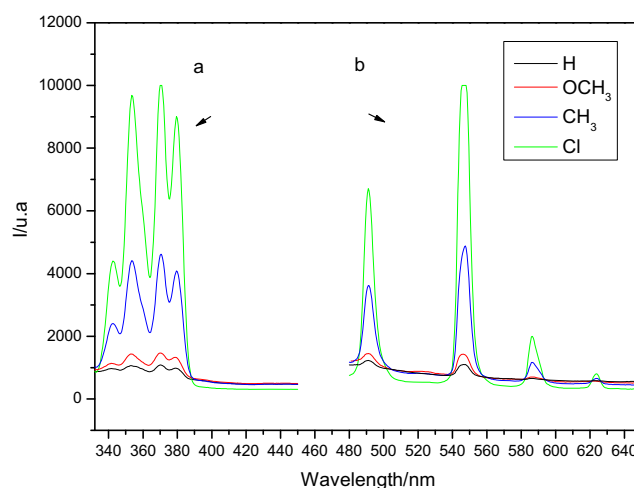


Fig. 8 Excitation (a) and emission (b) spectra of the complexes $[Tb(NO_3)_2 L^{1-4}]NO_3 \cdot 2H_2O$

of the central ions (Antenna effect). The sensitization involves placing lanthanide cations in proximity to chromophoric molecules having high absorptivity, and the closer the triplet state levels of the ligands to the emitting energy level of the central ions, the more efficient the intra-molecular energy transfer [16]. Among all ligands (L^{1-4}), L^4 substituted by $-Cl$, achieved energy transfer best, eventually the complex (RE = Eu, Tb) had the strongest intrinsic fluorescence than that of $[RE(NO_3)_2 L^{1-3}]NO_3 \cdot 2H_2O$. Meanwhile, the fluorescence intensity of $[RE(NO_3)_2 L^{2-4}]NO_3 \cdot 2H_2O$ substituted by $-CH_3$, $-OCH_3$, $-Cl$ was stronger than that of $[RE(NO_3)_2 L^1]NO_3 \cdot 2H_2O$, respectively, this was because that the substituent changed the electron cloud on the benzene ring, the energy level difference between the triplet state level of the ligands and the lowest excited state level of the central ions was changed, thus the emission intensity of the fluorescence was influenced.

By comparison between Eu(III) and Tb(III) complexes, the emission intensity of $[Tb(NO_3)_2 L^{2,4}]NO_3 \cdot 2H_2O$ were obviously stronger than that of $[Eu(NO_3)_2 L^{2,4}]NO_3 \cdot 2H_2O$, which deduced that the ligands $L^{2,4}$ had better energy level matching degree with lowest excited state of Tb^{3+} ion.

Electrochemical Properties

The electrochemical properties of rare earth (Eu, Tb) complexes were analyzed by the cyclic voltammetry (CV) in dimethyl sulfoxide solution. The highest occupied molecular orbit (HOMO, $E_{HOMO} = -(4.74 + E_{OX} - E_{Fc/Fc^+})$) and the lowest unoccupied molecular orbit (LUMO, $E_{LUMO} = E_{HOMO} + E_g$, $E_g = hc/\lambda_{onset} = 1240/\lambda_{onset}$) [17, 22] were obtained, as shown in Table 8. Since the cyclic voltammetry curves of all the complexes are similar, only the cyclic voltammetry curves of $[Eu(NO_3)_2 L^{1-4}]NO_3 \cdot 2H_2O$ are selected for illustration, as shown in Fig. 9.

Table 8 The HOMO and LUMO energy levels of the Eu^{3+} , Tb^{3+} complexes

Complex	λ_{onset} (nm)	E_{ox}^{a} (v)	E_{g}^{b} (eV)	$E_{\text{HOMO}}^{\text{c}}$ (eV)	$E_{\text{LUMO}}^{\text{d}}$ (eV)
$[\text{Eu}(\text{NO}_3)_2\text{L}^1]\text{NO}_3 \cdot 2\text{H}_2\text{O}$	256	0.537	4.844	−5.277	−0.433
$[\text{Eu}(\text{NO}_3)_2\text{L}^2]\text{NO}_3 \cdot 2\text{H}_2\text{O}$	256	0.404	4.844	−5.144	−0.300
$[\text{Eu}(\text{NO}_3)_2\text{L}^3]\text{NO}_3 \cdot 2\text{H}_2\text{O}$	256	0.466	4.844	−5.206	−0.362
$[\text{Eu}(\text{NO}_3)_2\text{L}^4]\text{NO}_3 \cdot 2\text{H}_2\text{O}$	256	0.667	4.844	−5.407	−0.563
$[\text{Tb}(\text{NO}_3)_2\text{L}^1]\text{NO}_3 \cdot 2\text{H}_2\text{O}$	255	0.568	4.863	−5.308	−0.445
$[\text{Tb}(\text{NO}_3)_2\text{L}^2]\text{NO}_3 \cdot 2\text{H}_2\text{O}$	256	0.518	4.844	−5.258	−0.414
$[\text{Tb}(\text{NO}_3)_2\text{L}^3]\text{NO}_3 \cdot 2\text{H}_2\text{O}$	257	0.508	4.825	−5.248	−0.423
$[\text{Tb}(\text{NO}_3)_2\text{L}^4]\text{NO}_3 \cdot 2\text{H}_2\text{O}$	257	0.667	4.825	−5.407	−0.582

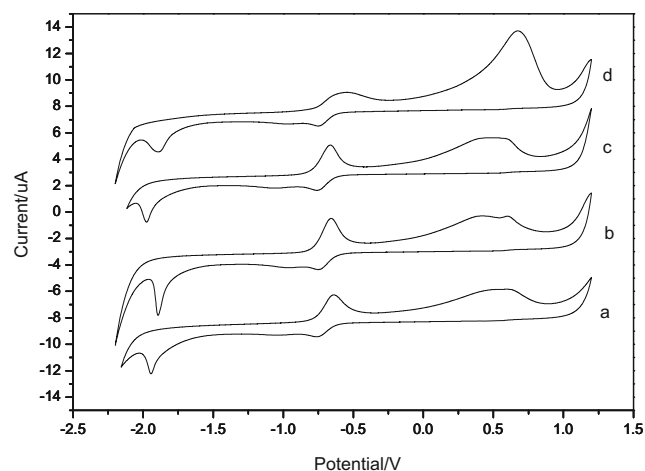
^a Oxidation potentials measured by cyclic voltammetry with ferrocene as the standard (the oxidation potential of ferrocene set as zero)

^b Band gap estimated from the UV–vis absorption spectrum

^c Calculated from the oxidation potentials

^d Deduced from the HOMO and E_{g}

From Table 8, it was obvious that the oxidation potential of rare earth $[\text{RE}(\text{NO}_3)_2\text{L}^4]\text{NO}_3 \cdot 2\text{H}_2\text{O}$ complexes was the highest than that of $[\text{RE}(\text{NO}_3)_2\text{L}^{1-3}]\text{NO}_3 \cdot 2\text{H}_2\text{O}$, while $[\text{RE}(\text{NO}_3)_2\text{L}^1]\text{NO}_3 \cdot 2\text{H}_2\text{O}$ was stronger than that of $[\text{RE}(\text{NO}_3)_2\text{L}^2, 3]\text{NO}_3 \cdot 2\text{H}_2\text{O}$, this mainly due to the influence of the substituent on the benzene ring. The introduction of electron-donating group ($-\text{CH}_3$, $-\text{OCH}_3$) to the ligand enhanced the ability of losing electrons, so the oxidation potentials were decreased. As for the L^4 , the inductive effect and conjugative effect of the substituent ($-\text{Cl}$) contributed to stabilizing the electron, so the oxidation potential was increased. Thus, the highest occupied molecular orbit were increased in the order $[\text{Eu}(\text{NO}_3)_2\text{L}^2]\text{NO}_3 \cdot 2\text{H}_2\text{O} < [\text{Eu}(\text{NO}_3)_2\text{L}^3]\text{NO}_3 \cdot 2\text{H}_2\text{O} < [\text{Eu}(\text{NO}_3)_2\text{L}^1]\text{NO}_3 \cdot 2\text{H}_2\text{O} < [\text{Eu}(\text{NO}_3)_2\text{L}^4]\text{NO}_3 \cdot 2\text{H}_2\text{O}$ and $[\text{Tb}(\text{NO}_3)_2\text{L}^3]\text{NO}_3 \cdot 2\text{H}_2\text{O} < [\text{Tb}(\text{NO}_3)_2\text{L}^2]\text{NO}_3 \cdot 2\text{H}_2\text{O} < [\text{Tb}(\text{NO}_3)_2\text{L}^1]\text{NO}_3 \cdot 2\text{H}_2\text{O} < [\text{Tb}(\text{NO}_3)_2\text{L}^4]\text{NO}_3 \cdot 2\text{H}_2\text{O}$.

**Fig. 9** Cyclic voltammetry curve of $[\text{Eu}(\text{NO}_3)_2\text{L}^{1-4}]\text{NO}_3 \cdot 2\text{H}_2\text{O}$ (a–d)

Conclusions

Solid complexes of rare earth (Eu, Tb) nitrate with Schiff base ligands were synthesized and characterized. The thermodynamic analysis showed that the starting decomposition temperatures of rare earth complexes were approximately 100 °C. The fluorescence analysis showed that the ligands L^{1-4} possessed excellent fluorescence properties and the emission intensity of L^4 was the strongest. The fluorescence intensity of rare earth (Eu, Tb) complexes were decreased in the order $[\text{RE}(\text{NO}_3)_2\text{L}^4]\text{NO}_3 \cdot 2\text{H}_2\text{O} > [\text{RE}(\text{NO}_3)_2\text{L}^2]\text{NO}_3 \cdot 2\text{H}_2\text{O} > [\text{RE}(\text{NO}_3)_2\text{L}^3]\text{NO}_3 \cdot 2\text{H}_2\text{O} > [\text{RE}(\text{NO}_3)_2\text{L}^1]\text{NO}_3 \cdot 2\text{H}_2\text{O}$ (RE = Eu, Tb). This tendency was attributed to the efficient intra-molecular energy transfer from the triplet state level of the ligands to the lowest excited state level of the central ions (Eu^{3+} , Tb^{3+}). The synthesized compounds showed three-primary colours, which may be significant for studying organic light-emitting device and fluorescence probe. The electrochemical properties of rare earth (Eu, Tb) complexes were also investigated. The results showed that the electron-donating group ($-\text{CH}_3$, $-\text{OCH}_3$) in ligands $\text{L}^{2,3}$ increased the highest occupied molecular orbit, while electron-withdrawing group ($-\text{Cl}$) in L^4 decreased.

Acknowledgments We are grateful to the financial support of the National Natural Science Foundation of China (No.J1103312; No.J1210040; No.21341010), the Innovative Research Team in University (No.IRT1238) and chemical excellent engineer training program of Hunan university. We also thank Dr. William Hickey, the U.S. professor of HRM, for the English editing on this paper.

References

- Gouveia-Neto AS, da Costa EB, Bueno LA, Ribeiro SJL (2004) Upconversion luminescence in transparent glass ceramics containing $\beta\text{-PbF}_2$ nanocrystals doped with erbium. *J Alloys Compd* 375: 224–228

2. Gandara F, Gutierrez-Puebla E, Iglesias M, Snejko N, Angeles Monge M (2010) Isolated hexanuclear hydroxo lanthanide secondary building units in a rare-earth polymeric framework based on p-sulfonatocalix[4]arene. *Cryst. Growth Des* 10:128–134
3. Tanabe S (2006) Optical properties and local structure of rare-earth-doped amplifier for broad band telecommunication. *J. Alloys Compd* 408–412:675–679
4. Fabbri P, Mohammad Poor S, Ferrari L, Rovati L, Borsacchi S, Geppi M, Lima PP, Carlos LD (2014) Highly stable plastic optical fibre amplifiers containing [Eu(btfa)₃(MeOH)(bpeta)]: a luminophore able to drive the synthesis of polyisocyanates. *Polym* 55:488–494
5. Mascharak PK (2002) Structural and functional models of nitrile hydratase. *Coord Chem Rev* 225:201–214
6. Gutierrez F, Tedeschi C, Maron L, Daudey JP, Poteau R, Azema J, Tisnès P, Picard C (2004) Quantum chemistry-based interpretations on the lowest triplet state of luminescent lanthanide complexes. Part 1. Relation between the triplet state energy of hydroxamate complexes and their luminescence properties. *J Chem Soc Dalton Trans* 9:1334–1347
7. Latva M, Takalob H, Mukkala VM, Matachescu C, Rodriguez-Ubis JC, Kankarea J (1997) Correlation between the lowest triplet state energy level of the ligand and lanthanide (III) luminescence quantum yield. *J Lumin* 75:149–169
8. Kanmani Raja K, Indra Gandhi N, Lekha L, Easwaramoorthy D, Rajagopal G (2014) Synthesis, spectral, electrochemical and catalytic properties of Ru(III) Schiff base complexes containing N, O donors. *J Mol Struct* 1060:49–57
9. Shi Q, Xu LJ, Ji JX, Li YM, Wang RH, Zhou ZY, Cao R, Hong MC, Chan ASC (2004) Syntheses and structures of two anion-templated dinuclear cadmium complexes with diamino-binaphthyl Schiff bases as ligands. *Inorg Chem Commun* 7:1254–1257
10. Okawa H, Furutachi H, Fenton DE (1998) Heterodinuclear metal complexes of phenol-based compartmental macrocycles. *Coord Chem Rev* 174:51–75
11. Sawodny WJ, Riederer M (1977) Addition compounds with polymeric chromium(II)-Schiff base complexes. *Angew Chem Int Ed Eng* 16:859–860
12. Taha ZA, Ajlouni AM, Al-Hassan KA, Hijazi AK, Faig AB (2011) Syntheses, characterization, biological activity and fluorescence properties of bis-(salicylaldehyde)-1,3-propylenediimine Schiff base ligand and its lanthanide complexes. *Spectrochim Acta A* 81317–323
13. Yoon II, Narita M, Shimizu T, Asakawa M (2004) Threading-followed-by-shrinking protocol for the synthesis of a [2]rotaxane incorporating a Pd(II) – salophen moiety. *J Am Chem Soc* 126:16740–16741
14. Liu YH, He W, Yang ZH, Chen YW, Wang XW, Guo DC (2015) Synthesis, characterization and properties of novel amide derivatives based open-chain crown ether and their Tb (III) complexes. *J Lumin* 160:35–42
15. Eldehna WM, Ibrahim HS, Abdel-Aziz HA, Farrag NN, Youssef MM (2015) Design, synthesis and in vitro antitumor activity of novel N-substituted-4-phenyl/benzylphthalazin-1-ones. *Eur J Med Chem* 89:549–560
16. Sato S, Wada M (1970) Relations between intramolecular energy transfer efficiencies and triplet state energies in rare earth β -diketone chelates. *Bull Chem Soc Jpn* 43:1955–1962
17. Bard AJ, Memming R, Miller B (1991) Terminology in semiconductor electrochemistry and photoelectrochemical energy conversion. *Pure Appl Chem* 63:569–596
18. Kirby AF, Richardson FS (1983) Detailed analysis of the optical absorption and emission spectra of europium(3+) in the trigonal (C₃) Eu(DBM)₃.H₂O system. *J Phys Chem* 87:2544–2556
19. Meng DF, Liu F, Lian XM, Yang ZH, Guo DC (2014) Synthesis and properties of salicylaldehyde salicylhydrazon derivatives and their europium complexes. *J Fluoresc* 24:1661–1669
20. Geary WJ (1971) The use of conductivity measurements in organic solvents for the characterisation of coordination compounds. *Coord Chem Rev* 7:81–122
21. Qiang S (1993) Chemistry of rare earths. Henan Technology & Science Press, Zhengzhou, pp. 304–314 (in Chinese)
22. Trasatti S (1986) The absolute electrode potential: an explanatory note. *Pure Appl Chem* 58:955–966